Available online at www.sciencedirect.com
ScienceDirect
Trans. Nonferrous Met. Soc. China 26(2016) 697−703
Transactions of Nonferrous Metals Society of China
www.tnmsc.cn

Effects of Li addition on microstructure and mechanical properties of Mg−6Al−2Sn−0.4Mn alloys

Yong-Ho KIM[1], Hyeon-Taek SON[1,2]

1. Automotive Component & Materials R&BD Group, Korea Institute of Industrial Technology, Gwangju 61012, Korea;
2. Department of Rare Metals Engineering, University of Science & Technology, Daejeon 34113, Korea

Received 22 April 2015; accepted 31 October 2015

Abstract: Effects of Li addition (2%, 5%, 8% and 11%) on microstructure and mechanical properties of the as-cast and as-extruded Mg−6Al−2Sn−0.4Mn-based alloys were investigated. Mg−*x*Li−6Al−2Sn−0.4Mn (*x*= 2, 5, 8 and 11, mass fraction, %) alloys were cast under an SF_6 and CO_2 atmosphere at 700 ℃. After homogenization heat treatment at 350 ℃, cast billets were extruded with a reduction ratio of 40:1 at 200 ℃. Li addition to Mg−6Al−2Sn−0.4Mn resulted in the formation of $MgSnLi_2$ and $MgAlLi_2$ and/or AlLi intermetallic compounds and random basal texture. With increasing Li addition, β-Li phase was increased and the average area fraction of precipitates increased. Compression yield strength was increased from 212 to 235, 242 and 239 MPa as Li content was increased from 2% to 5%, 8% and 11%, respectively. Elongation was remarkably increased above 60% in 11% Li alloy. It is probable that Li-containing phases play a significant role in the enhanced mechanical properties by Li addition.
Key words: magnesium alloy; Li addition; extrusion; microstructure; mechanical property

1 Introduction

Mg alloys are considered as potential candidates for numerous applications, especially transportation vehicles or electric components owing to low density (1.74 g/cm^3), excellent damping capacity and high specific strength. However, the poor plastic formability due to hexagonal close-packed (HCP) structure limits the applications of Mg. Therefore, the development of new Mg alloys with high formability is an important issue to improve the manufacturing ability. Among Mg alloy, Li addition in Mg alloy systems results in the transformation of the crystal structure from HCP to body-centered cubic (BCC) with more slip system [1−3]. According to the binary Mg−Li phase diagram, when the Li content lies between 5.7% and 11%, the BCC structured β phase will co-exist with the HCP structured α phase. These Mg−Li alloys are exceptionally light-weighted since Li has a density of only 0.53 g/cm^3. Therefore, Mg−Li alloys have advantages of ultra-light weight with a specific gravity and good formability at room temperature. However, these alloys exhibit relatively low strength, which restricts their practical engineering applications. Hence, it is an important matter to improve the mechanical properties of the Mg−Li alloys. Recently, many researchers have studied the mechanical properties of Mg−Li alloys, including the effects of severe deformation processes, addition of alloying elements and precipitation hardening [4−7]. In order to improve mechanical property, various alloying elements have been added to Mg−Li alloy systems. Among Mg−Li alloy systems, Al and Zn were the most widely used elements in alloying process due to the formation of metastable $MgAlLi_2$ and $MgZnLi_2$ in these alloys [8−10]. Recently, Sn addition to Mg−Li alloys results in the improvement of mechanical properties due to grain refinement and newly formed $MgSnLi_2$ phase together with Mg_2Sn phase, via the effective blockage of dislocation motion [11,12]. The alloying element Mn to Mg alloys is helpful in refining the grain size and improving the tensile strength.

The current work was conducted to investigate the effects of Li addition on the microstructure and mechanical properties of the as-cast and extruded Mg−6Al−2Sn−0.4Mn-based alloys.

2 Experimental

The compositions of the four studied alloys are

Corresponding author: Hyeon-Taek SON; Tel: +82-62-6006310; E-mail: sht50@kitech.re.kr
DOI: 10.1016/S1003-6326(16)64160-2

Mg−*x*Li−6Al−2Sn−0.4Mn (*x*=2, 5, 8 and 11, mass fraction, %). Commercially pure Mg, Li, Al, and Sn were used to prepare these alloys, and manganese (Mn) was added as Mg−5%Mn master alloy. The Mg−*x*Li−6Al−2Sn−0.4Mn (*x*=2, 5, 8 and 11) alloys were cast under SF_6 and CO_2 atmosphere in a steel crucible. The alloy melts were cast into a steel mold (75 mm in diameter, 250 mm in height), which was heated at 200 ℃, at a pouring temperature of 700 ℃. Then, the cast billets (70 mm in diameter, 100 mm in height) were homogenized at 350 ℃ for 4 h and water-cooled. After the as-homogenized billets were held at 200 ℃ for 1 h, the extrusion was carried out with a reduction ratio of 40:1. The diameter of the extruded bar was 12 mm. Then, the microstructures of as-extruded alloys were examined by an optical microscope (OM, Nikon), and a scanning electron microscope (SEM, JSM7000F) equipped with an electron backscatter diffraction (EBSD) system. Phase analyses were performed using X-ray diffractometer (XRD) with a resource of Cu K_α radiation. Samples were cut and ground mechanically into a mirror-like surface using abrasive papers and diamond pastes. Compression tests were performed using a universal material test machine (SHIMAZU AG-IS) at room temperature. The mechanical tests were carried out at an initial strain rate of 1.0×10^{-3} s^{-1}.

3 Results and discussion

Figure 1 shows the optical micrographs of the as-cast Mg−*x*Li−6Al−2Sn−0.4Mn alloys (*x*=2, 5, 8 and 11). It can be seen that the microstructures strongly depend on the Li content of the alloys. In the as-cast 2% and 5% Li-containing alloys (Figs. 1(a) and (b)), a dendritic microstructure was observed. With increasing Li content to 8% and 11%, *β*-Li phase increased and *α*-Mg phase decreased as shown in Figs. 1(c)−(f). The as-cast microstructure of the 5%, 8% and 11% Li-containing alloys exhibited a dual phase of *α*-Mg and *β*-Li structure. In the 8% Li alloy (Figs. 1(c) and (e)),

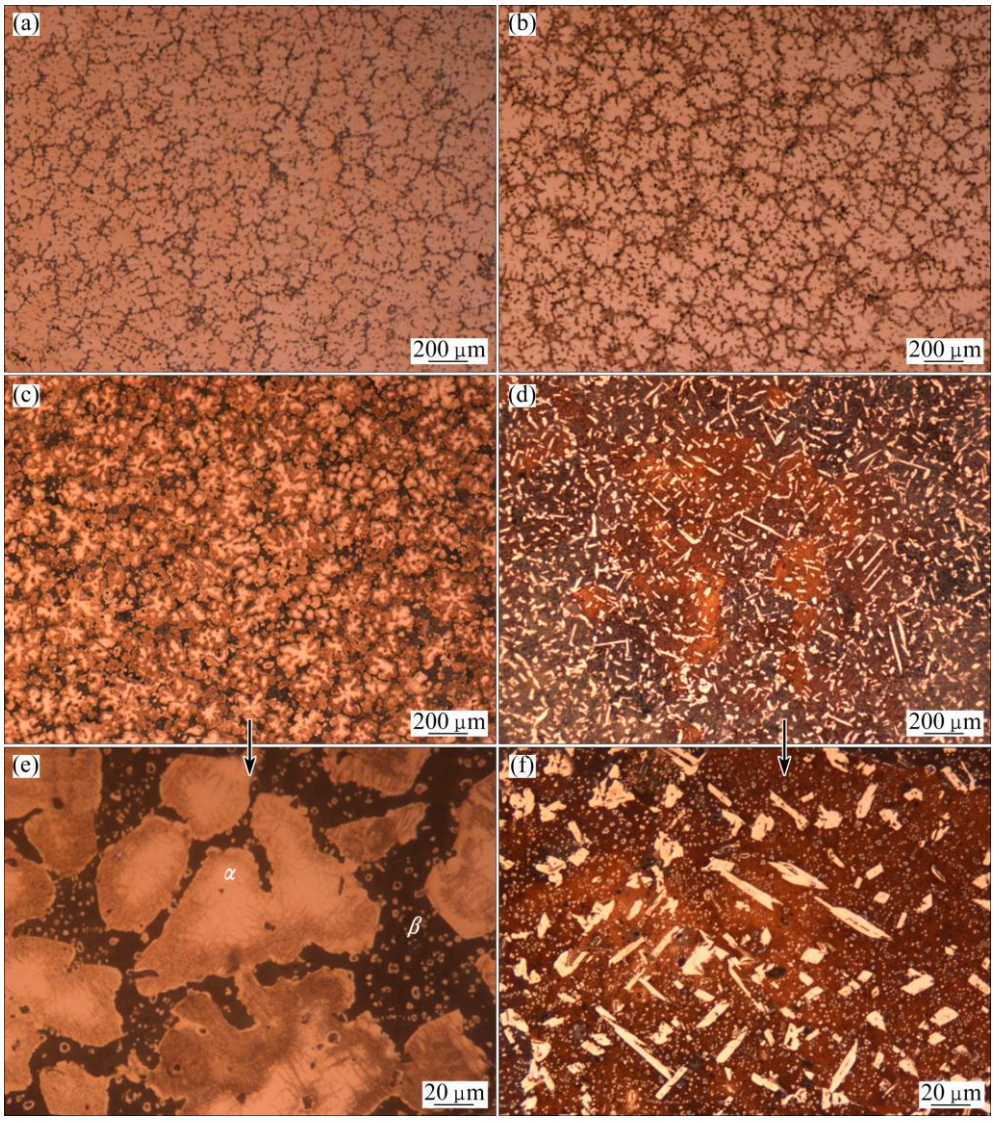

Fig. 1 Optical micrographs of as-cast Mg−*x*Li−6Al−2Sn−0.4Mn alloys: (a) *x*=2; (b) *x*=5; (c, e) *x*=8; (d, f) *x*=11

dendritic α-Mg phase was surrounded by β-Li phase. On the other hand, needle type α-Mg phase was observed in the as-cast 11%Li-containing alloy as shown in Figs. 1(d) and (f).

Figure 2 shows the SEM-BEI images of the as-cast Mg−xLi−6Al−2Sn−0.4Mn alloys (x=2, 5, 8 and 11). Microstructures of the as-cast alloys exhibited three kinds of major phases such as dark, grey and bright contrast. Microstructure of the 2% Li addition alloy consisted of α-Mg phase and precipitates. Whereas, microstructures of the 5%, 8% and 11% Li addition alloys comprised α-Mg phase, β-Li phase and precipitates. In order to examine the average area fraction of the phases, image analyses were conducted from SEM-BEI images of as-cast alloys with different Li contents as shown in Table 1. As Li contents increased from 2% to 5%, 8% and 11%, the average area fractions of the α-Mg phase were decreased from 97.50% to 86.62%, 67.33% and 22.41%, while the average area fractions of β-Li phase were increased from 0 to 10.16%, 27.77% and 70.89%, respectively. All as-cast Li-containing alloys have many precipitates in the α-Mg and β-Li phases. Moreover, the average area fraction of precipitates was increased from 2.5% to 3.23%, 4.90% and 6.7% by increasing Li addition from 2% to 5%, 8% and 11%.

The X-ray diffraction patterns of the Li-containing alloys in the as-cast condition are depicted in Fig. 3. Similar to the results mentioned above, with the increasing Li content of the alloys, the intensity of the β-Li phase was increased, whereas that of the α-Mg phase was decreased. Therefore, microstructures of 5%, 8% and 11%Li-containing alloys presented a dual phase of α-Mg phase and the β-Li phase. Only α-Mg phase was observed in the 2%Li-containing alloy. In addition, Li addition to Mg−6Al−2Sn−0.4Mn alloy resulted in the formation of $MgSnLi_2$, $MgAlLi_2$ and/or AlLi intermetallic compounds as shown in Fig. 4. According to SEM and XRD analyses, the coarse precipitate was identified as the $MgSnLi_2$ intermetallic compounds. On the other hand, the fine precipitate distributing β-Li phase was confirmed as $MgAlLi_2$ and/or AlLi

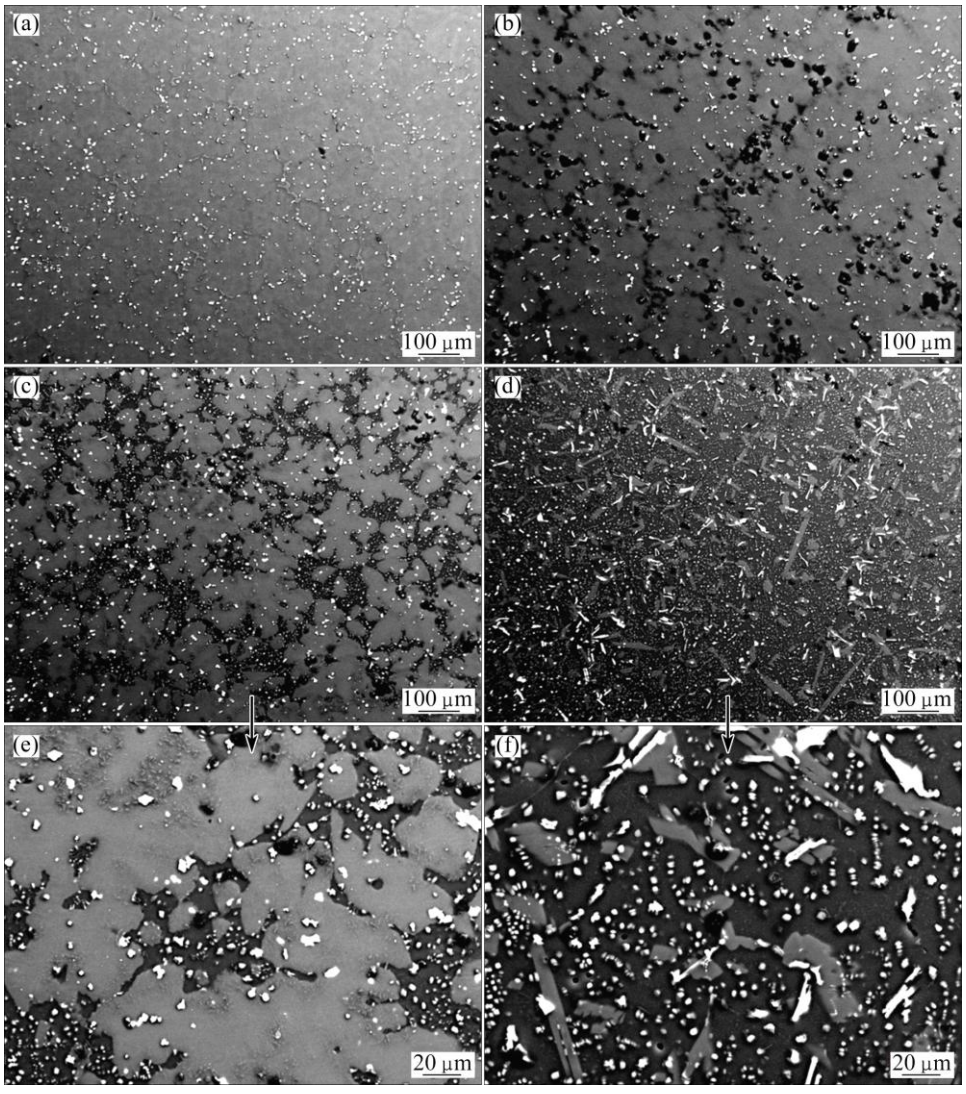

Fig. 2 SEM-BEI images of as-cast Mg−xLi−6Al−2Sn−0.4Mn alloys: (a) x=2; (b) x=5; (c, e) x=8; (d, f) x=11

Table 1 Average area fractions of phases taken from SEM-BEI images of as-cast Mg−*x*Li−6Al−2Sn−0.4Mn alloys

Alloy	Average area fraction/%		
	α-Mg	β-Li	Precipitate
Mg−6Al−2Sn−0.4Mn−2Li	97.50	−	2.50
Mg−6Al−2Sn−0.4Mn−5Li	86.62	10.16	3.22
Mg−6Al−2Sn−0.4Mn−8Li	67.33	27.77	4.90
Mg−6Al−2Sn−0.4Mn−11Li	22.41	70.89	6.70

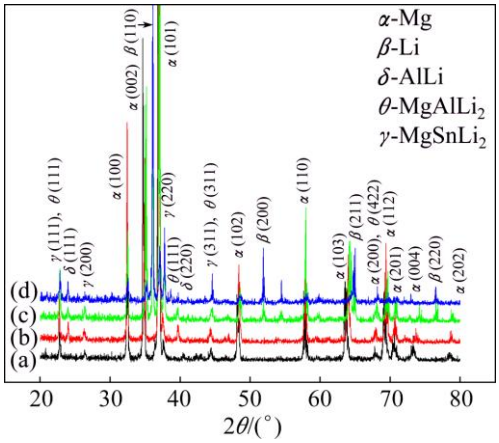

Fig. 3 XRD patterns of as-cast Mg−*x*Li−6Al−2Sn−0.4Mn alloys: (a) *x*=2; (b) *x*=5; (c) *x*=8; (d) *x*=11

intermetallic compounds. In particular, during solidification of the 8% and 11% Li addition alloys with α-Mg and β-Li phases, primary precipitate is $MgSnLi_2$ intermetallic compound. The primary precipitates act like a nucleation site for α-Mg. The presence of primary precipitates within the β-phase region can be attributed to the thickening of the dendrites which push these types of precipitates from dendrites to interdentritic region. As temperature reduces, the secondary $MgAlLi_2$ and/or AlLi precipitates form in the β-phase region. Therefore, it may be inferred that needle type α-Mg phase is related to the formation of $MgAlLi_2$ and/or AlLi precipitates in the β-phase region.

Figure 4 shows the optical micrographs of the as-extruded Mg−*x*Li−6Al−2Sn−0.4Mn alloys (*x*=2, 5, 8 and 11). It is apparent that the microstructure is arranged approximately parallel to the extrusion direction. In the 8% and 11% Li-containing alloys, the α-Mg and β-Li phases with the lamellar structure were elongated to the extrusion direction as shown in Figs. 4(c) and (d).

In order to observe the detailed microstructure of the as-extruded Mg−*x*Li−6Al−2Sn−0.4Mn alloys, SEM-BEI analyses were conducted as shown in Fig. 5. The as-extruded alloys were composed of α-Mg phase with the light gray, β-Li phase with the dark gray and precipitates with the bright. With increasing Li content, a fraction of precipitates was increased. Moreover, coarse needle-type $MgSnLi_2$ intermetallic compound of the extruded 11% Li-containing alloy showing as-cast microstructure was fragmented to fine particles with polygon shape due to severe deformation during hot extrusion, as shown in Fig. 5(d).

Figure 6 shows EBSD maps and pole figures of the as-extruded Mg−*x*Li−6Al−2Sn−0.4Mn alloys obtained

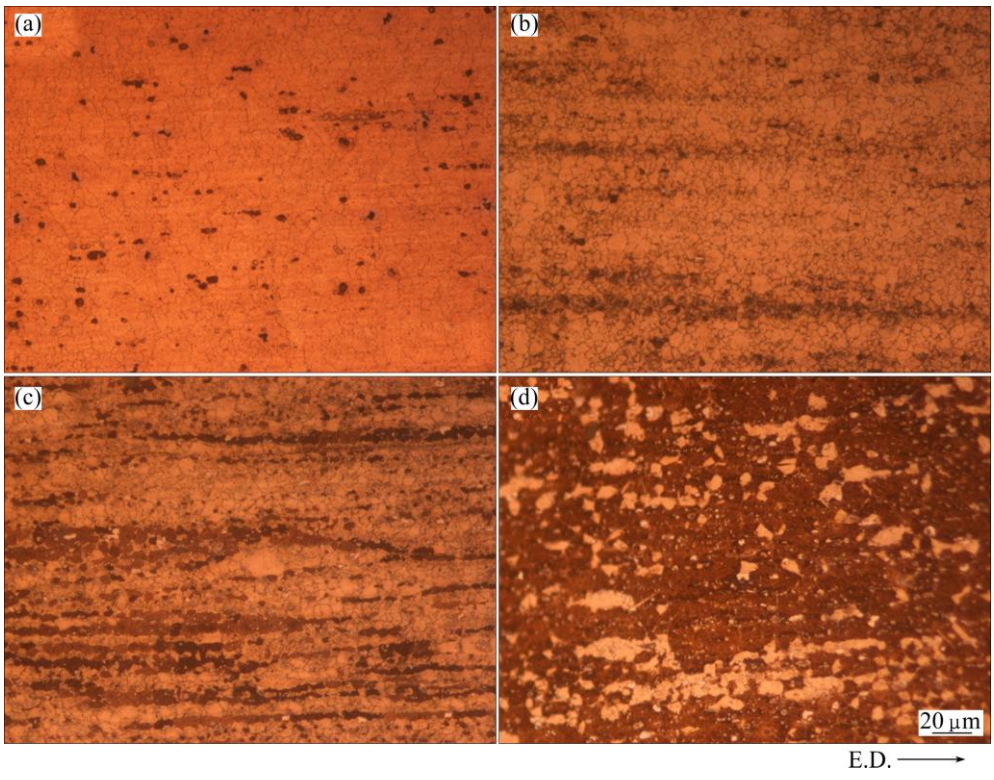

Fig. 4 Optical micrographs of as-extruded Mg−*x*Li−6Al−2Sn−0.4Mn alloys: (a) *x*=2; (b) *x*=5; (c) *x*=8; (d) *x*=11%

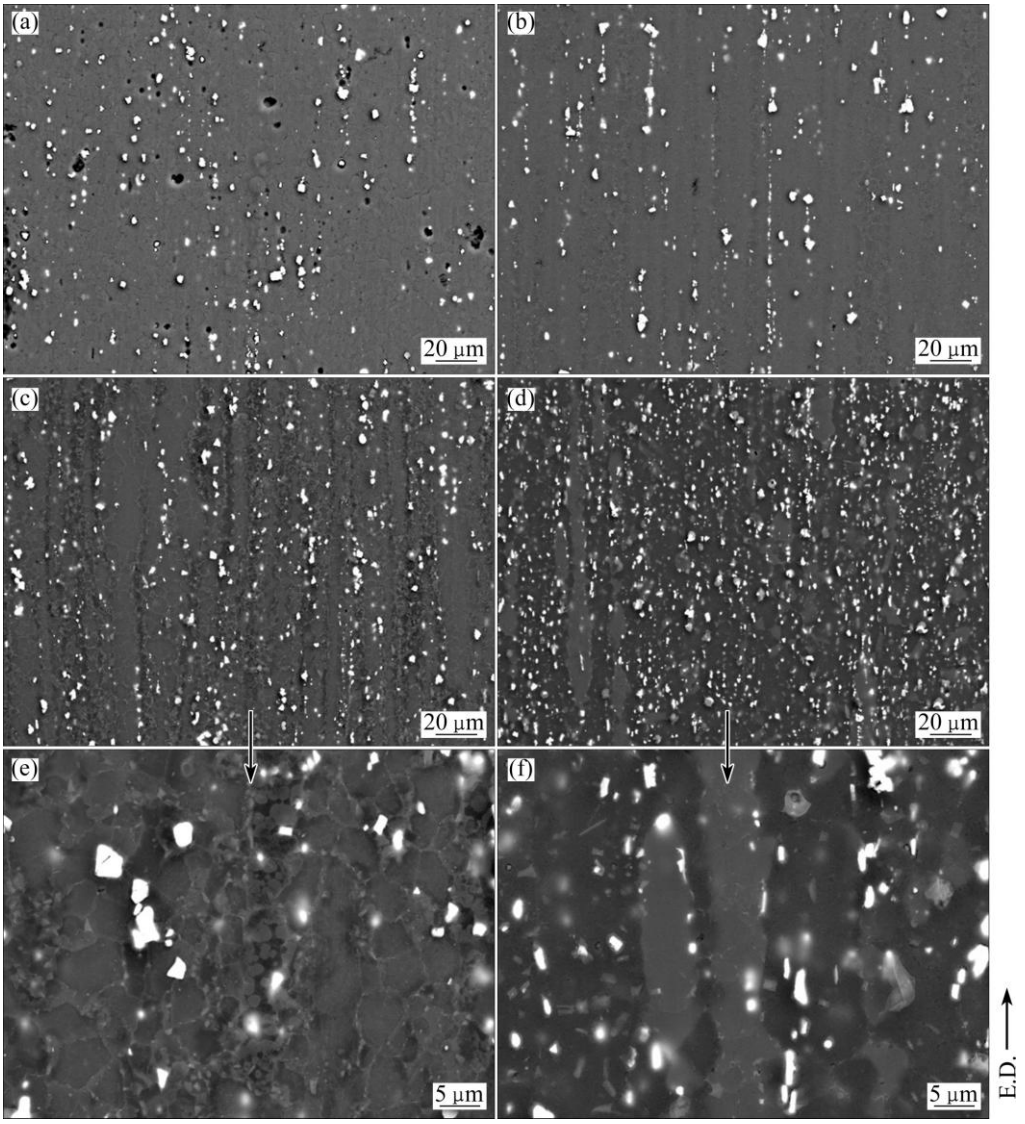

Fig. 5 SEM-BEI images of as-extruded Mg−*x*Li−6Al−2Sn−0.4Mn alloys: (a) *x*=2; (b) *x*=5; (c, e) *x*=8; (d, f) *x*=11

from parallel section to extrusion direction. The *β*-phase could not be analyzed due to the formation of the surface oxidation in the high Li content. Therefore, EBSD analyses were obtained from only *α*-Mg phase. With increasing Li addition from 0 to 2%, 5%, 8% and 11%, the average grain sizes of the *α*-Mg matrix were remarkably decreased from 12.20 to 6.36 to 3.61, 4.22 and 4.23 μm. Maximum intensity of (0002) basal plane was decreased from 6.655 to 4.406, 3.96, 3.745 and 3.858 with increasing Li addition from 0 to 2%, 5%, 8% and 11% as shown in Figs. 6(f), (g), (h), (i) and (j). Obviously, all alloys with Li addition have a random basal texture and weaker peak intensity of (0002) plane compared with Mg−6Al−2Al−2Sn−0.4Mn (no Li addition). It is considered that Li addition to Mg−6Al−2Sn−0.4Mn alloys resulted in the development of the random texture. The weakened basal texture by Li addition has been also associated with the particle stimulated nucleation (PSN) of dynamic recrystallization during extrusion [14]. $MgSnLi_2$, $MgAlLi_2$ and AlLi precipitates can increase the driving force for recrystallization and act as nucleation sites. In addition, Li addition is attributed to the weaker (0002) basal texture due to formation of non-basal slip such as prismatic or pyramidal slip by reduction of the (*c*/*a*) ratio. In *α*-Mg phase, maximum (0002) intensity of alloys with 5%, 8% and 11%Li was of similar value due to similar (*c*/*a*) ratio by maximum solid solubility of 5.7% Li in *α*-Mg phase.

Figure 7 shows compression and tensile stress curves of the as-extruded Mg−*x*Li−6Al−2Sn−0.4Mn alloys at room temperature (*x*=2, 5, 8 and 11). Compression yield strength was increased from 212 to 235, 242 and 239 MPa as Li content was increased from 2% to 5%, 8% and 11% due to the increase of volume fraction of the precipitates and grain refinement. Also, maximum compression strength was increased. Li addition to Mg−6Al−2Sn−0.4Mn resulted in the

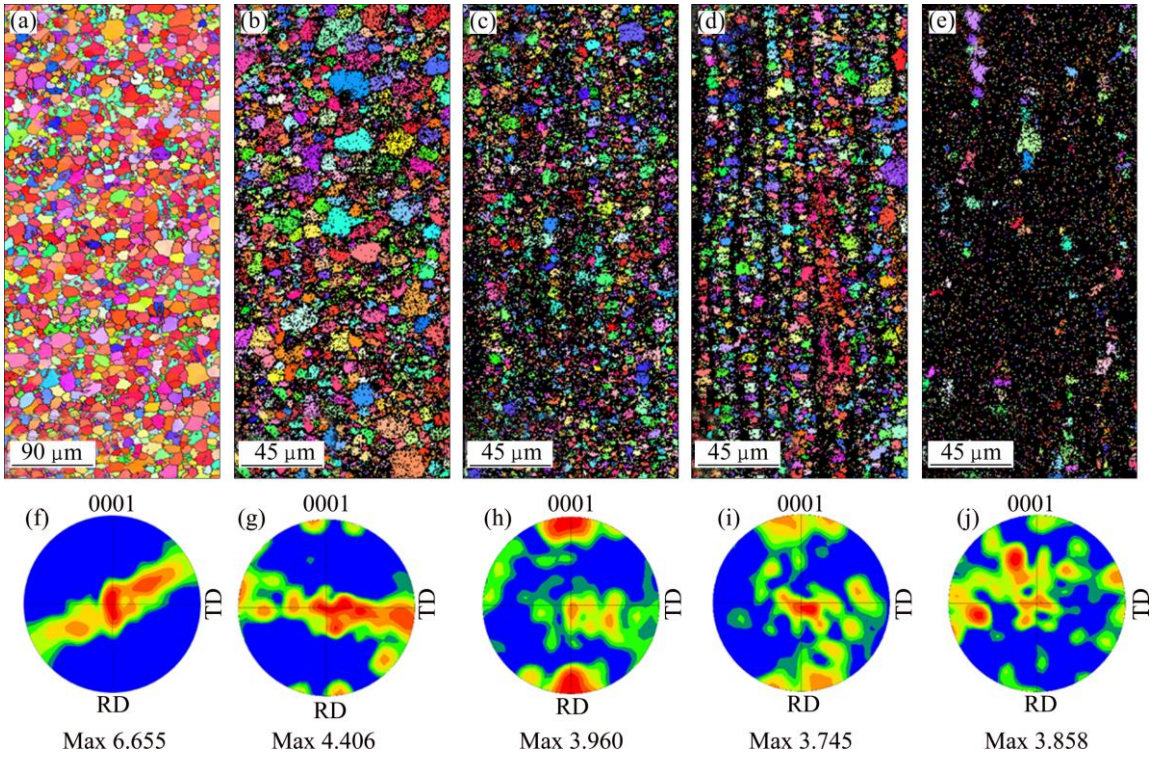

Fig. 6 EBSD maps and PFs taken parallel to extrusion direction in as-extruded Mg−*x*Li−6Al−2Sn−0.4Mn alloys: (a) *x*=0; (b) *x*=2; (c) *x*=5; (d) *x*=8; (e) *x*=11

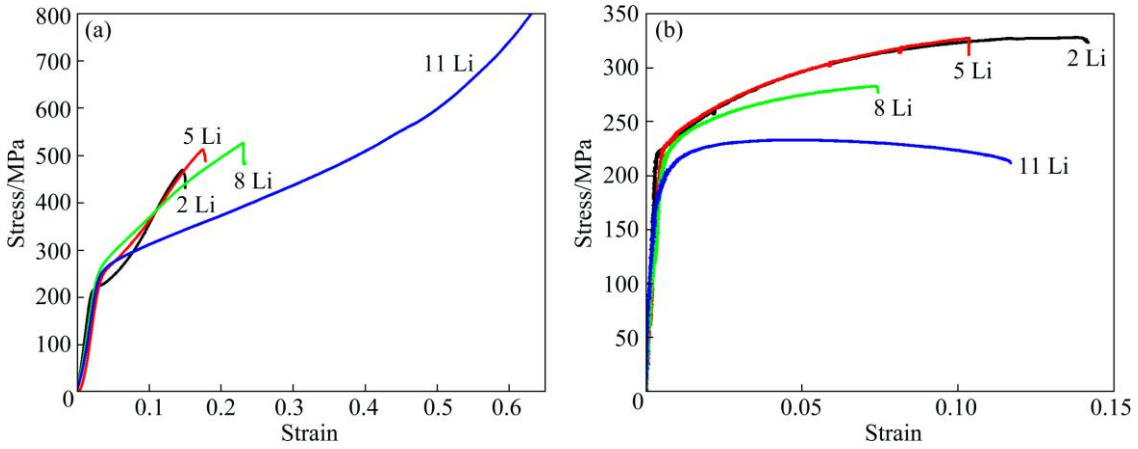

Fig. 7 Nominal compression (a) and tensile (b) stress−strain curves of as-extruded Mg−*x*Li−6Al−2Sn−0.4Mn alloys

formation of the $MgSnLi_2$, $MgAlLi_2$ and/or AlLi intermetallic compounds and these particles play an important role in the improvement of strength due to providing effective barriers to gliding dislocations during deformation. With the increase of Li addition from 2% to 5% and 8%, elongation was increased from 14.6% to 17.4% and 23.0%. In particular, elongation of the 11% Li- containing alloy was remarkably improved to above 60%. During the compression test deformation of 60%, fracture did not occur. Clearly, it is noted that Li addition to Mg−6Al−2Sn−0.4Mn alloys resulted in the improvement of elongation due to the increase of volume fraction of β-phase (BCC crystal structure). On the other hand, tensile yield strength was decreased from 225 MPa to 229, 216, and 188 MPa with the increase of Li addition from 2% to 5% and 8%. Tensile elongation was decreased from 14.1% to 10.3%, 7.4% and 11.6% although Li content was increased. It is considered that decrease of strength and elongation was related to the formation of precipitates in interface region of α and β phases.

4 Conclusions

In this research, effects of Li addition on microstructure and mechanical properties of the

hot-extruded Mg−6Al−2Sn−0.4Mn-based alloys have been investigated. As Li contents increased from 2% to 5%, 8% and 11%, the average area fractions of the α-Mg phase were decreased from 97.50% to 86.62%, 67.33% and 22.41%, while the average area fractions of β-Li phase were increased from 0 to 10.16%, 27.77% and 70.89%, respectively. The average area fractions of precipitates were increased from 2.5% to 3.23%, 4.90% and 6.7%. Li addition to Mg−6Al−2Sn−0.4Mn alloy resulted in the formation of $MgSnLi_2$, $MgAlLi_2$ and/or AlLi intermetallic compounds and the development of the random texture. Compression yield strengths were increased from 212 to 235, 242 and 239 MPa as Li content was increased from 2% to 5%, 8% and 11% due to the increase of volume fraction of the precipitates and grain refinement. With the increase of Li addition from 2% to 5% and 8%, elongation was increased from 14.6% to 17.4% and 23.0%. In particular, elongation of the 11%Li-containing alloy was remarkably improved to above 60% at room temperature due to transformation from HCP to BCC crystal structure and a weaker basal texture.

References

[1] KAMADO S, KOJIMA Y. Deformability and strengthening of superlight Mg−Li alloys [J]. Materials Science and Technology, 1998, 14: 45−54.

[2] YAMAMOTO A, ASHIDA T, KOUTA Y, KIM K B, FUKUMOTO S, TSUBAKINO H. Microstructural characterization of a Mg−9%Li−1%Zn Alloy [J]. Materials Transactions, 2003, 44: 619−624.

[3] TAKUDA H, MATSUSAKA H, KIKUCHI S, KUBOTA K. Tensile properties of a few Mg−Li−Zn alloy thin sheets [J]. Journal of Materials Science, 2002, 37: 51−57.

[4] ZENG Ying, JIANG Bin, ZHANG Ming-xing, YIN Heng-mei, LI Rui-hong, PAN Fu-sheng. Effect of $Mg_{24}Y_5$ intermetallic particles on grain refinement of Mg−9Li alloy [J]. Intermetallics, 2014, 45: 18−23.

[5] GUPTA A, KUMAR V, NAIR J, BANSAL A, BALANI K. Abridgment of nano and micro length scale mechanical properties of novel Mg−9Li−7Al−1Sn and Mg−9Li−5Al−3Sn−1Zn alloys using object oriented finite element modeling [J]. Journal of Alloys and Compounds, 2015, 634: 24−31.

[6] XU D K, ZU T T, YIN M, XU Y B, HAN E H. Mechanical properties of the icosahedral phase reinforced duplex Mg−Li alloy both at room and elevated temperatures [J]. Journal of Alloys and Compounds, 2014, 582: 161−166.

[7] LV Bin-jiang, PENG Jian, WANG Yong-jian, AN Xiao-qin, ZHONG Li-ping, TANG Ai-tao, PAN Fu-sheng. Dynamic recrystallization behavior and hot workability of Mg−2.0Zn−0.3Zr−0.9Y alloy by using hot compression test [J]. Materials and Design, 2014, 53: 357−365.

[8] JIANG Bin, QU Zhi-kun, WU Rui-zhi, ZHANG Mi-lin. The solution and room temperature aging behavior of Mg−9Li−xAl(x=3, 6) alloys [J]. Journal of Alloys and Compounds, 2012, 536: 145−149.

[9] XU Tian-cai, PENG Xiao-dong, JIANG Jun-wei, XIE Wei-dong, CHEN Yuan-fang, WEI Guo-bing. Effect of Sr content on microstructure and mechanical properties of Mg−Li−Al−Mn alloy [J]. Transactions of Nonferrous Metals Society of China, 2014, 24(9): 2752−2760.

[10] SON Hyeon-Taek, KIM Yong-Ho, KIM Dae-Won, KIM Jung-Han, YU Hyo-Sang. Effects of Li addition on the microstructure and mechanical properties of Mg−3Zn−1Sn−0.4Mn based alloys [J]. Journal of Alloys and Compounds, 2013, 564: 130−137.

[11] JIANG Yan, CHEN Yu-an, FANG Dan, JIN Li. Effect of Li on microstructure, mechanical properties and fracture mechanism of as-cast Mg−5Sn alloy [J]. Materials Science and Engineering A, 2015, 641: 256−262.

[12] JIANG Bin, ZENG Ying, ZHANG Ming-xing, YIN Heng-mei, YANG Qing-shan, PAN Fu-sheng. Effects of Sn on microstructure of as-cast and as-extruded Mg−9Li alloys [J]. Transactions of Nonferrous Metals Society of China, 2013, 23(4): 904−908.

[13] KUMAR V, GOVIND, SHEKHAR R, BALASUBRAMANIAM R, BALANI K. Microstructure evolution and texture development in thermomechanically processed Mg−Li−Al based alloys [J]. Materials Science and Engineering A, 2012, 547: 38−50.

[14] ROBSON J D, HENRY D T, DAVIS B. Particle effects on recrystallization in magnesium–manganese alloys [J]. Acta Materialia, 57, 2009, 9: 2739−2747.

锂添加对 Mg−6Al−2Sn−0.4Mn 合金显微组织和力学性能的影响

Yong-Ho KIM[1], Hyeon-Taek SON[1,2]

1. Automotive Component & Materials R&BD Group, Korea Institute of Industrial Technology, Gwangju 61012, Korea;
2. Department of Rare Metals Engineering, University of Science & Technology, Daejeon 34113, Korea

摘　要：研究添加 2%、5%、8%和 11%锂对铸态和挤压态 Mg−6Al−2Sn−0.4Mn 合金的显微组织和力学性能的影响。在 SF_6 和 CO_2 气氛和 700 ℃ 温度下铸造 Mg−xLi−6Al−2Sn−0.4Mn(x=2，5，8 和 11 质量分数，%)合金。经 350 ℃ 均匀化热处理后，铸锭在 200 ℃ 进行挤压，挤压比为 40:1。在 Mg−6Al−2Sn−0.4Mn 合金中添加锂可以形成 $MgSnLi_2$，$MgAlLi_2$ 和/或 AlLi 金属间化合物以及随机基面织构。随着锂含量的增加，β-Li 相增加且沉淀相的平均面积分数也增加。随着锂含量从 2%增加至 5%、8%和 11%，合金的抗压屈服强度从 212 MPa 分别增加至 235、242 和 239 MPa。 当锂含量达到 11%时，合金的伸长率超过 60%。锂添加对含锂相合金力学性能的提高起到重要作用。

关键词：镁合金；锂添加；挤压；显微组织；力学性能

(Edited by Yun-bin HE)